Hydrodynamics of stratified epithelium: Steady state and linearized dynamics

Wei-Ting Yeh[1,2,*] and Hsuan-Yi Chen[1,2,3,†]
[1]*Department of Physics, National Central University, Jhongli 32001, Taiwan*
[2]*Institute of Physics, Academia Sinica, Taipei 11529, Taiwan*
[3]*Physics Division, National Center for Theoretical Sciences, Hsinchu 30013, Taiwan*
(Received 25 February 2016; published 31 May 2016)

A theoretical model for stratified epithelium is presented. The viscoelastic properties of the tissue are assumed to be dependent on the spatial distribution of proliferative and differentiated cells. Based on this assumption, a hydrodynamic description of tissue dynamics at the long-wavelength, long-time limit is developed, and the analysis reveals important insights into the dynamics of an epithelium close to its steady state. When the proliferative cells occupy a thin region close to the basal membrane, the relaxation rate towards the steady state is enhanced by cell division and cell apoptosis. On the other hand, when the region where proliferative cells reside becomes sufficiently thick, a flow induced by cell apoptosis close to the apical surface enhances small perturbations. This destabilizing mechanism is general for continuous self-renewal multilayered tissues; it could be related to the origin of certain tissue morphology, tumor growth, and the development pattern.

DOI: 10.1103/PhysRevE.93.052421

I. INTRODUCTION

Biological tissues are viscoelastic. Concepts developed to describe passive viscoelastic materials have been applied to biological tissues [1,2]. However, active processes such as forces generated by the cells, cell movement, and cell proliferation make biological tissues different from passive viscoelastic materials. Thus biological tissues fall into the category of active soft matter [3]. On the other hand, junctions between neighboring cells prevent free diffusion of cells in a tissue. This makes biological tissues different from other active biological systems such as bacterial colonies and cell cytoplasm. As a result, biological tissues become interesting systems for study of complex collective motion and morphogenesis. For example, it is known that the homeostasis state of a tissue often has an undulating surface to increase the contact area with its environment. Understanding the formation and maintenance of this spatial structure is thus important for fundamental research of active matter and for applied research such as fabricating functional surfaces and flexible electronics [4].

Experiments have demonstrated that at short time scales a tissue is solid-like due to the adhesion junctions between cells [5]. Since the residual stresses can relax due to turnover of junction proteins [2,6] and cell rearrangement induced by cell division and cell apoptosis [7], a tissue is liquid-like at long time scales [1,2,8–11]. This suggests a characteristic time τ such that at time scales smaller than τ a tissue behaves like a solid with shear modulus E. On the other hand, at time scales larger than τ, a tissue behaves like a fluid with viscosity η. Typically, $E \sim 10^2$–10^4 Pa [10] and $\tau \sim 10$–10^2 s [8,10], therefore $\eta = E\tau$ is of the order of 10^3–10^6 Pa s [12].

In this study we focus on stratified epithelium, a multilayered continuous self-renewal tissue [13]. Epithelium often forms the outermost layer of skin and mucous membrane and acts as a barrier separating the outside and inside of a multicellular organism [14]. On the top of a stratified epithelium is a free apical surface; on the bottom is a basement membrane attached to the underlying connective tissue composed primarily of collagen and elastin fibers. Typically the thickness of the stratified epithelium is $\sim$100 μm and the thickness of the underlying connective tissue is $\sim$1 mm [15]. The proliferative cells are often localized near the basal lamina, suggesting the existence of a special microenvironment called the stem cell niche [16,17]. Above the proliferative cells are terminally differentiated (TD) cells. They are functional cells that do not divide; instead they undergo programmed cell death (apoptosis). Intuitively, different cells should have different mechanical properties. As supported by recent experiments, stem cells and tumor cells often have a lower stiffness than normal differentiated cells [18,19]. This suggests that the mechanical properties of a tissue should also depend on the local tissue composition [7]. The effects of such inhomogeneity on tissue dynamics is the focus of this study.

Undulating or fingering structures that are important for biological functions are often seen in the apical surface or basal membrane of a stratified epithelium. For example, skin wrinkles or folds are formed when a skin is deformed by external or residual stresses with a wavelength of $\sim$ 1 mm [15,20–22]. At the length scale of $\sim$100 μm, rete pegs interdigitating with dermal papillae are observed in the interface between skin epithelium and stroma [23–25]. Similar structures have also been observed in the epithelium of mucous membrane [20,26–28]. Studies have shown that elastic forces could be important during the formation of the aforementioned structures. By modeling a stratified epithelium as an elastic solid in contact with the underlying elastic connective tissue, the formation of skin wrinkles was associated with a buckling instability originating from the competition between the bending energy of epithelium and the stretching energy of connective tissue [15,21]. The rete peg structure was suggested to arise from the incompatible growth of epithelium and connective tissue [29]. A similar mechanism can also explain the formation of fingerprint [30], crypt [31], and surface wrinkling of tumor spheroids [32]. On the other hand, hydrodynamic instabilities are also likely to produce undulating morphologies in stratified

*wtyeh1989@gmail.com
†hschen@phy.ncu.edu.tw

epithelium. For example, the formation of a rete peg structure can arise from proliferation-induced stresses [33], and an essential condition of this result is that the net cell proliferative rate deceases with the distance from the basal lamina. Some models have considered more details such as the cell lineage dynamics [34], viscoelasticity of the underlying stroma [35], and effect of growth factors inside a tissue [34,35]. Overall, several interesting structures and patterns can be understood by a continuum description of tissues without describing the movement of individual cells and biomolecular events in detail. The mechanical stresses induced by cell turnover inside a tissue [7,12] are sufficient to do this job.

The aim of this work is to study theoretically how inhomogeneity of mechanical properties in a tissue affects tissue dynamics. For illustrative purposes we consider a stratified epithelium on a rigid stroma. We begin with a simple model in which the mechanical properties of the tissue are assumed to be homogeneous. With proliferative cells occupying the lower part and TD cells occupying the upper part of the tissue, this model has a homeostasis state with a flat apical surface. The linearized dynamics close to the homeostasis state in this model already reveals interesting effects from flows and cell proliferation. For example, cell division or apoptosis speeds up tissue relaxation towards the homeostasis state, but this effect is relatively weak when the wavelength of the perturbation is of the order of the thickness of the tissue.

Due to frequent cell division events, tissue viscosity in the region rich in proliferative cells should be different from that in the rest of the tissue. This feature is included in our second model. We find that this modification can lead to different tissue dynamics close to the homeostasis state. Especially, when the proliferative region becomes sufficiently thick, cell apoptosis close to the apical region can induce a flow that strongly hinders the relaxation towards the steady state. This effect is especially significant for perturbations with a wavelength comparable to the tissue thickness ($\sim$100 μm for typical stratified epithelium). Since our model is quite general, we expect this destabilizing mechanism to exist in continuous self-renewal tissue, but it is not easy to observe in normal healthy tissue because the proliferative cells occupy only a thin region. However, during development or regeneration there is often a transient increase in proliferative cells inside a tissue [36]. As a result, the new effect described by our second model can occur, and it is possible that an undulating apical surface could be generated by this mechanism.

This article is organized as follows. Both models are presented in Sec. II, where we also discuss the steady states and linearized dynamics close to the steady states. In Sec. III we discuss the flow in an epithelium that is induced by cell division or apoptosis. Using the result derived in Appendix B, we also discuss the relation between the dimensionless parameter $r_{\rm rel} = r_D/r_S$ and $\eta_{\rm rel} = \eta_D/\eta_S$, where r_D and r_S are the cell apoptosis rate and cell division rate, and η_D and η_S are the viscosities in the regions rich in differentiated cells and proliferative cells, respectively. In Sec. IV, based on these results, we draw a conclusion and propose possible experimental tests to validate our theory. Appendix A presents the calculation of the growth rate of a small perturbation in our second model. A derivation of the tissue viscosity from a hydrodynamic model is presented in Appendix B.

II. MODELS

A. First model: Stratified epithelium with a constant viscosity

Consider a basel lamina sitting on the xy plane. An epithelium grows from this surface into the $z > 0$ region. On top of the epithelium is a free apical surface. We are interested in the steady state of this system and the linearized dynamics close to this steady state. Since epithelial growth typically takes several days to complete [23,24], in this article we focus on the long-time behavior of our model. Therefore processes with a relaxation time not longer than the time scale τ introduced in Sec. I have all decayed away. The elasticity of the tissue can be neglected, and the tissue behaves as a viscous fluid [8–11]. The viscosity of the tissue depends on cell-turnover events [7] and the rearrangement of junction proteins [2,6]. Experimentally, the viscosity of a tissue can be estimated from the elastic constant E and relaxation time τ through the relation $\eta = E\tau$.

Since the dynamics is slow, the inertia of the tissue is also negligible. Imposing incompresibility for simplicity, the equation of continuity, force balance, and constitutitive equation are [33,35]

$$\partial_l v_l = k_p, \tag{1}$$

$$\partial_i \sigma_{ik} = 0, \tag{2}$$

$$\sigma_{ik} = -p\delta_{ik} + 2\eta v_{ik}. \tag{3}$$

Here v_i is the ith component of the flow velocity field, $v_{ik} \equiv (\partial_i v_k + \partial_k v_i)/2$ is the strain rate tensor in the tissue, p is the tissue pressure, η is the viscosity of the tissue, and k_p is the (net) cell proliferation rate in the tissue. In general, k_p is a decreasing function of z because both nutrient and proliferative cells are relatively abundant near the basal lamina. In our first model, η is chosen to be a constant for simplicity.

We focus on the situation where the tissue is soft compared to the stroma, therefore the stroma is modeled as a rigid substrate for simplicity, and the flow field vanishes at $z = 0$. A more general model that includes the viscoelastic properties of the stroma will be deferred to future studies. The flow field and stress at the apical surface of the tissue satisfy the free boundary condition, which includes contributions from the surface tension of the tissue and external pressure.

The steady-state velocity field of Eqs. (1)–(3) with these boundary conditions is

$$v_x^* = v_y^* = 0 \quad \text{and} \quad v_z^*(z) = \int_0^z k_p(z')dz'. \tag{4}$$

A superscript asterisk (*) is used to denote steady-state values. Since v_z^* should vanish at the apical surface, we have the steady-state condition

$$0 = \int_0^{H^*} k_p(z)dz, \tag{5}$$

where H^* is the thickness of the tissue in the steady state. Since k_p is a decreasing function of z, for the solution of Eq. (5) to exist, the tissue needs to have $k_p(0) > 0$ and $k_p(H^*) < 0$. Intuitively, this means that cell division events in the lower part of the tissue should be balanced by cell apoptosis in the upper part of the tissue.

A homeostasis state of a tissue is a steady state that is stable against small perturbations. To check whether the steady state in this model corresponds to a homeostasis state, we consider a perturbation that takes the tissue height from H^* to $H(x,t) = H^* + \delta H(x,t)$. Similarly, $v_k = v_k^* + \delta v_k$, $p = p^* + \delta p$, etc. The linearized equations for the perturbed system are

$$\partial_l \delta v_l = 0 \tag{6}$$

and

$$-\partial_k \delta p + \eta \partial_l \partial_l \delta v_k = 0. \tag{7}$$

Note that the perturbed tissue is assumed to be translationally invariant in the y direction.

For a perturbation with $\delta H \sim e^{iqx+\omega t}$, the no-slip boundary condition at $z = 0$ gives $\delta v_x|_{z=0} = \delta v_z|_{z=0} = 0$. The linearized boundary conditions at $z = H^*$ are

$$-\delta p|_{z=H^*} + 2\eta \partial_z \delta v_z|_{z=H^*} = \sigma \partial_x \partial_x \delta H \tag{8}$$

and

$$\eta(\partial_z \delta v_x|_{z=H^*} + \partial_x \delta v_z|_{z=H^*}) = -2\eta k_p(H^*)\partial_x \delta H, \tag{9}$$

where σ is the surface tension of the apical surface. The above two equations describe the stress balance in the normal and tangential directions of the apical surface, respectively. There is also a linearized kinematic boundary condition connecting the evolution of the tissue surface and the flow field:

$$\partial_t \delta H = \delta v_z|_{z=H^*} + k_p(H^*)\delta H. \tag{10}$$

The dispersion relation $\omega(q)$ of the growth rate of the perturbation can be calculated from Eqs. (6)–(10); straightforward algebra that is described in Appendix A gives

$$\omega(q) = \omega_{\text{mech}}(q) + \omega_{\text{phy}}(q). \tag{11}$$

The first term,

$$\omega_{\text{mech}} = \frac{2qH^* - \sinh 2qH^*}{2(qH^*)^2 + (1+\cosh 2qH^*)} \frac{\sigma q}{2\eta} \equiv K^{\text{I}}_{\text{mech}}(qH^*)\frac{\sigma q}{2\eta}, \tag{12}$$

is the same as the dispersion relation for the surface of a low-Reynolds-number simple fluid. In the limit of large qH^* this term approaches $-\sigma q/2\eta$ [37]. As Fig. 1 shows, $K^{\text{I}}_{\text{mech}}$ is negative for all q; this means that the surface tension of the apical surface tends to stabilize the steady state. The second term is

$$\omega_{\text{phy}} = \frac{1+\cosh(2qH^*)}{2(qH^*)^2 + 1 + \cosh(2qH^*)} k_p(H^*) \equiv K^{\text{I}}_{\text{phy}}(qH^*)|k_p(H^*)|. \tag{13}$$

ω_{phy} and $K^{\text{I}}_{\text{phy}}$ are always negative since $k_p(H^*) < 0$, i.e., the apical region of the tissue is rich in TD cells, which do not divide but undergo apoptosis. The meaning of this term is intuitive: cell proliferation and cell apoptosis help to bring a perturbed tissue back to the steady state. Note that for given $k_p(H^*)$, $|\omega_{\text{phy}}|$ has a minimum at wave number $q = \Xi/H^*$, where Ξ is the solution of $\cosh \Xi = \Xi \sinh \Xi$. Numerically one finds that $\Xi \cong 1.2$ and $\omega_{\text{phy}}(q = \Xi/H^*) \cong 0.7k_p(H^*)$.

In this simple model, it is convenient to think that the relaxation of the tissue towards the steady state is due to apical surface tension and cell proliferation. The contribution from surface tension grows as the wave number q of the perturbation increases; the contribution from cell proliferation is relatively weak when $qH^* \sim \mathcal{O}(1)$. We emphasize that our model is independent of the details of $k_p(z)$; the only constraint for $k_p(z)$ is that the steady-state tissue height H^* which satisfies Eq. (5) should be finite.

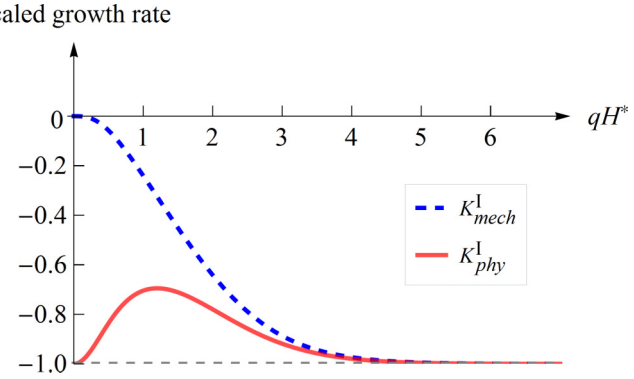

FIG. 1. $K^{\text{I}}_{\text{mech}}$ (dashed blue curve) and $K^{\text{I}}_{\text{phy}}$ (solid red curve). $K^{\text{I}}_{\text{mech}}$ decreases monotonically towards -1; $|K^{\text{I}}_{\text{phy}}|$ has a minimum at $qH^* \sim 1$.

B. Second model: Effect of viscosity heterogeneity

In a typical stratified epithelium, proliferative cells are located close to the basal region [16,17]. Due to their low abundance, typically the division rate of proliferative cells is high compared to the apoptosis rate of differentiated cells [38]. Since stress relaxation in a tissue strongly depends on the division and apoptosis of the cells [7], the viscosity in regions rich in proliferative cells should be lower than the viscosity in other regions of the tissue.

To consider position-dependent viscosity we assume that all proliferative cells reside in the region $z < h_S$, and differentiated cells are located at $z > h_S$. This is clearly an oversimplification; nevertheless, it captures the basic tissue composition in a stratified epithelium. The net cell proliferation rate inside the tissue is simply $k_p = r_S$ for $z < h_S$ and $k_p = -r_D$ for $z > h_S$. Here r_S is the cell division rate and r_D is the cell apoptosis rate. From Eq. (5), the proportion of the proliferative region in the steady state is related to r_S and r_D by

$$\frac{h_S}{H^*} = \frac{r_{\text{rel}}}{1 + r_{\text{rel}}}, \tag{14}$$

where $r_{\text{rel}} \equiv r_D/r_S$.

It is important to further discuss the connection between Eq. (14) and experiments, especially how the steady-state tissue height H^* can be controlled experimentally by tuning the magnitude of r_{rel} or h_S. In experiments r_{rel} can be controlled by changing the apoptosis rate of differentiated cells [39]. Furthermore, the height of the proliferative region h_S can be controlled by the density profile of certain signaling molecules (such as growth factor) [35]. Suppose these signaling molecules are generated in the $z < 0$ region, after which they permeate through the basal membrane and diffuse into the tissue; then a cell can determine its distance from the basal membrane by detecting the concentration of signaling molecules around it.

Based on this information, a cell can decide whether it should differentiate into a nonproliferative cell. Therefore h_S can be controlled by tuning the concentration profile of such signaling molecules.

With the aforementioned simplification for tissue composition, in our second model we assume that the viscosity in the tissue is $\eta = \eta_S$ for $z < h_S$ and $\eta = \eta_D$ for $z > h_S$. The geometry and boundary conditions for the linearized tissue evolution equations are the same as those for our first model, except for additional velocity and stress continuity conditions at $z = h_S$. The flow field in the steady state of our second model therefore becomes

$$v_x^* = v_y^* = 0$$

and

$$v_z^* = \begin{cases} r_S z & \text{for} \quad z < h_S, \\ r_S h_S - r_D(z - h_S) & \text{for} \quad h_S < z < H^*. \end{cases} \tag{15}$$

That is, the steady-state flow in the tissue is upward everywhere due to cell turnover, and the flow field is strong close to $z = h_S$. The continuity of normal stress at h_S leads to a discontinuity of tissue pressure in our model that should be smoothed out in a real tissue because the boundary between the proliferative region and the differentiated region is diffuse, not infinitely sharp.

Now let us consider a perturbation that changes the thickness of the tissue a little bit from the steady state. To make the analysis simple, we assume that cell differentiation happens whenever a cell moves upward to the $z > h_S$ region, therefore h_S is not affected by this perturbation. From the calculation discussed in Appendix A for the linearized dynamics around the steady state, for $\delta H \sim e^{iqx+\omega t}$ the growth rate ω of the perturbation in our second model can still be expressed as the sum of two terms, $\omega_{\rm mech}$ and $\omega_{\rm phy}$, but these two terms are very different from their counterparts in our first model. Let

$$\omega_{\rm mech} = K^{\rm II}_{\rm mech}(qH^*, r_{\rm rel}, \eta_{\rm rel})\frac{\sigma q}{2\eta_D}, \tag{16}$$

$$\omega_{\rm phy} = K^{\rm II}_{\rm hy}(qH^*, r_{\rm rel}, \eta_{\rm rel})|k_p(H^*)|, \tag{17}$$

where $\eta_{\rm rel} \equiv \eta_D/\eta_S$ and $k_p(H^*) = -r_D$. The analytical expressions of the dimensionless functions $K^{\rm II}_{\rm mech}$ and $K^{\rm II}_{\rm phy}$ are pretty complicated; they are shown in Eqs. (A9) and (A10) in Appendix A. In Fig. 2 we show how they change with qH^*, $\eta_{\rm rel}$, and $r_{\rm rel}$. Besides their shapes, it is important to note two issues. First, when $\eta_{\rm rel} = 1$ Eqs. (16) and (17) reduce to Eqs. (12) and (13) as we expected. This is illustrated in Figs. 2(a) and 2(c). Second, when $q = 0$ and $q \to \infty$, $\omega_{\rm phy}$ goes to $-|k_p(H^*)|$, this can be seen by taking proper limits for qH^* in Eq. (A10).

It is shown in Fig. 2(a) that $K^{\rm II}_{\rm mech}$ is always negative (stabilizing). Figure 2(b) shows that $|K^{\rm II}_{\rm mech}|$ increases with $r_{\rm rel}$; this is because as $r_{\rm rel}$ increases the thickness of the lower (less viscous) region of the tissue increases and there is less damping. Figure 2(c) shows that for given $r_{\rm rel}$ and $\eta_{\rm rel}$, $K^{\rm II}_{\rm phy}$ has

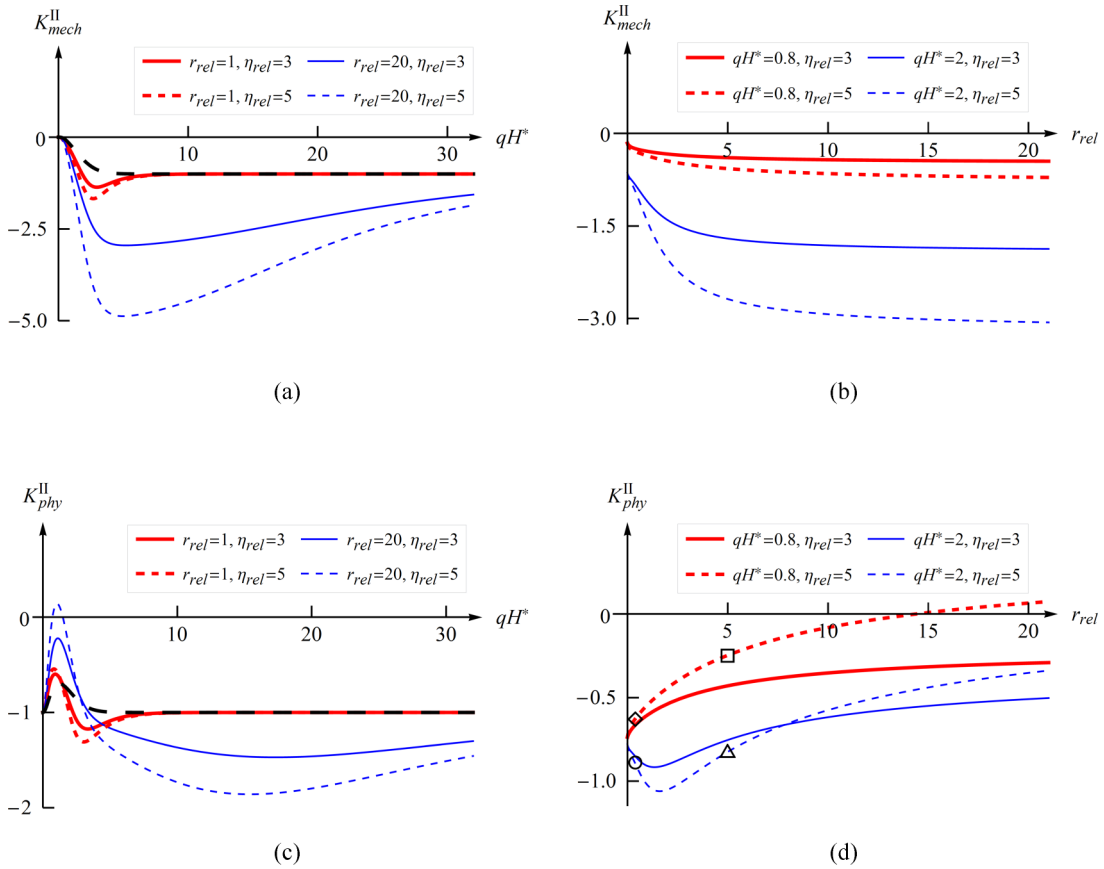

FIG. 2. (a) $K^{\rm II}_{\rm mech}$ versus qH^*. The long-dashed black curve is $K^{\rm I}_{\rm mech}$. (b) $K^{\rm II}_{\rm mech}$ versus $r_{\rm rel}$. (c) $K^{\rm II}_{\rm phy}$ versus qH^*. The long-dashed black curve is $K^{\rm I}_{\rm phy}$. (d) $K^{\rm II}_{\rm phy}$ versus $r_{\rm rel}$. The field lines of the deviatoric flows for parameters corresponding to those indicated by the open diamond, square, circle, and triangle are shown in Figs. 4(a)–4(d), respectively.

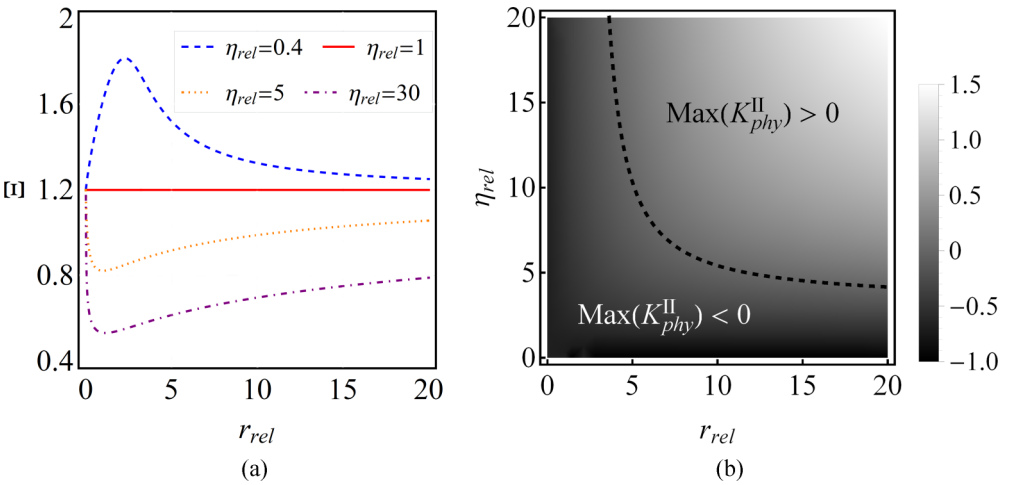

FIG. 3. (a) Ξ versus $r_{\rm rel}$ for $\eta_{\rm rel} = 0.4$ (long-dashed curve), $\eta_{\rm rel} = 1$ (solid curve), $\eta_{\rm rel} = 5$ (short-dashed curve), and $\eta_{\rm rel} = 30$ (dash-dotted curve). (b) The maximum $K^{\rm II}_{\rm phy}$ for a given $r_{\rm rel}$ and $\eta_{\rm rel}$, i.e., $K^{\rm II}_{\rm phy}(qH^* = \Xi, r_{\rm rel}, \eta_{\rm rel})$. The dotted curve shows where $K_{\rm phy}(qH^* = \Xi, r_{\rm rel}, \eta_{\rm rel}) = 0$.

a maximum at $qH^* = \Xi(r_{\rm rel}, \eta_{\rm rel})$. Figure 2(d) shows that $K^{\rm II}_{\rm phy}$ can be a nonmonotonic function of $r_{\rm rel}$. Since $K^{\rm II}_{\rm phy}$ originates from cell division or apoptosis, it cannot be explained solely by the viscous properties of the tissue. In the next section the flow field in the tissue is discussed in more detail, and the behavior of $K^{\rm II}_{\rm phy}$ can be better understood.

Figure 3(a) shows the position of the peak Ξ in Fig. 2(c) versus $r_{\rm rel}$ for different choices of $\eta_{\rm rel}$. In this figure it is clear that the maximum of $\omega_{\rm phy}$ occurs at $qH^* \sim \mathcal{O}(1)$. Figure 3(b) shows that when $r_{\rm rel}$ and $\eta_{\rm rel}$ are large, it is possible for $K^{\rm II}_{\rm phy}$ to be positive. That is, it is possible for cell division or apoptosis either to slow down the relaxation toward the steady state or to drive the tissue to an instability.

It is helpful to list the important results of our second model:

(i) In the limit $\eta_{\rm rel} \to 1$, our second model gives the same apical surface dispersion relation as our first model.

(ii) Apical surface tension tends to stabilize the steady state; this is similar to the results in our first model. This stabilizing effect is weaker as $r_{\rm rel}$ increases due to the greater proportion of the less viscous layer composed of proliferative cells.

(iii) When plotted against qH^*, $K^{\rm II}_{\rm phy}$ has a maximum at $qH^* = \Xi(r_{\rm rel}, \eta_{\rm rel})$. The magnitude of Ξ is of order unity.

(iv) The contribution from cell proliferation ($K^{\rm II}_{\rm phy}$) can be a nonmonotonic function of $r_{\rm rel}$. This is discussed in detail later.

(v) When both $r_{\rm rel}$ and $\eta_{\rm rel}$ are large, $K^{\rm II}_{\rm phy}$ can become positive. This is also discussed in detail later.

III. DISCUSSION

A. Flow induced by cell apoptosis on the apical surface

An important question of our hydrodynamic theory of epithelium tissue is, Besides fluidizing the tissue, how does cell turnover inside the tissue affect tissue dynamics? Let us begin our discussion by considering how the steady state of a tissue is maintained, and how a tissue evolves when its thickness is perturbed.

In the steady state, proliferative cells divide from time to time; because they are located relatively close to the basal membrane, the daughter cells are pushed upward. This upward flux of cells, described by Eq. (4) in our first model and Eq. (15) in our second model, replaces the loss due to the death of differentiated cells. This is described in the steady-state solutions of both our models,

When the tissue thickness is subject to a $q = 0$ perturbation, i.e., $H = H^* + \delta H(t)$, where $\delta H(t)$ is independent of x, the total number of differentiated cells is different from its steady-state value. When $\delta H > 0$ the excess differentiated cells lead to more cell apoptosis events per unit time in the tissue. Since h_S is fixed, the number of proliferative cells is not affected by δH; the total number of cells in the tissue decreases until δH goes back to 0. Similarly, when $\delta H < 0$ there are fewer cell apoptosis events in the tissue, which makes the tissue grow back to steady state. This is the simple intuitive picture that one can imagine without going through the analysis presented in the previous section. In our first model, one can see from Eqs. (12) and (13) that for $q = 0$ there is no contribution from apical surface tension, i.e., $\omega_{\rm mech}|_{q=0} = 0$, and the contribution from cell turnover gives a growth rate of the perturbation $\omega = \omega_{\rm phy}|_{q=0} = k_p(H^*) < 0$. This negative growth rate comes solely from the change in the number of cell death events per unit time due to tissue height change. The same behavior can be found for our second model from Eqs. (16), (17), (A9), and (A10). Thus our models support the simple intuitive picture.

When perturbation has $q \neq 0$, the contribution from $\omega_{\rm mech}$ is still easy to understand; it represents the contribution of the apical surface tension to the evolution of the perturbation. Because the apical surface tension tends to bring the tissue apical surface back to flat, this term always stabilizes the steady state. On the other hand, the contribution from $\omega_{\rm phy}$ is not trivial. In the first model tissue viscosity is assumed to be homogeneous; Fig. 1 shows that $\omega_{\rm phy}$ always tends to stabilize the steady state but its effect is relatively weak when $qH^* \sim 1$. In the second model $\omega_{\rm phy}$ can help the growth of perturbations with $qH^* \sim 1$, as long as $r_{\rm rel}$ and $\eta_{\rm rel}$ are sufficiently large (Fig. 3).

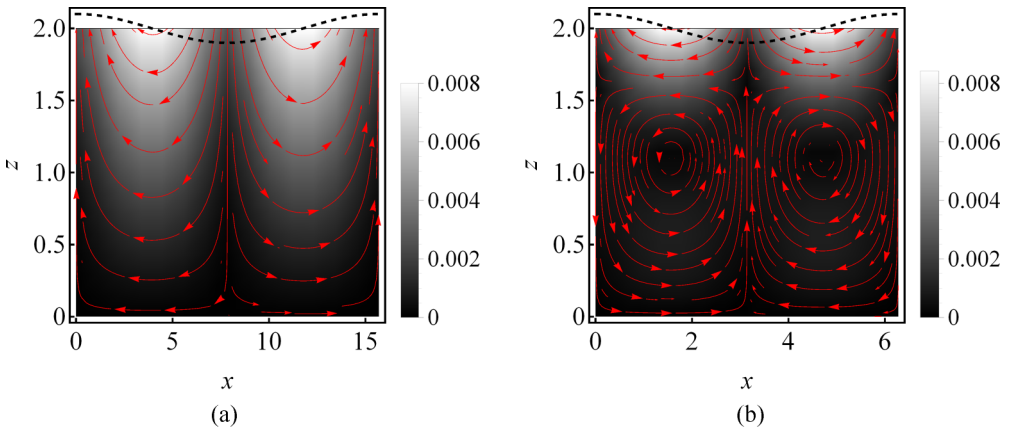

FIG. 4. (a, b) Field lines of $(\delta v_x, \delta v_y)$ at $t = 0$ calculated from our first model for a perturbed tissue with tissue apical surface tension $\sigma = 0$. $qH^* = 0.8$ $(qH^* < \Xi)$ in (a); $qH^* = 2$ $(qH^* > \Xi)$ in (b). The width along the x axis is chosen to be one wavelength. Red arrows are the stream lines, dashed black lines are the apical surface of the perturbed tissue, and the background gray level indicates the magnitude of δv. Flow fields are taken from the solution of the linearized dynamics for $k_p(H^*) = -1$, $H^* = 2$, and $\delta H(t = 0) = 0.01\cos(qx)$.

To see how perturbation with nonzero q gives rise to such nontrivial behavior, especially when the tissue viscosity depends on the distance from the basal surface, let us now consider a tissue with zero apical surface tension. Since there is no surface tension, cell turnover is the only driving force that generates flow in the tissue, and $(\delta v_x, \delta v_y)$, the deviation of the velocity field from steady state, is the difference between the flow due to cell turnover in a tissue with a perturbed surface height and the flow in a tissue in its steady state. In other words, $(\delta v_x, \delta v_y)$ in a tissue with zero apical tension can help us to illuminate the mechanism that makes $\omega_{\rm phy}|_{q\neq 0}$ different from $\omega_{\rm phy}|_{q=0}$. From the solutions of the linearized dynamics presented in Sec. II, we plot the field lines of $(\delta v_x, \delta v_y)$ at $t = 0$ for our first model in Fig. 4. The field lines of $(\delta v_x, \delta v_y)$ at $t = 0$ for our second model are presented in Fig. 5.

Figures 4 and 5 show that when qH^* is larger than Ξ, the magnitude of δv rapidly decays as one moves away from the apical surface, therefore it is reasonable to expect that when qH^* is large, $\omega_{\rm phy}|_{q\neq 0}$ gradually approaches $\omega_{\rm phy}|_{q=0}$. Indeed, this can also be found by checking the analytical expressions of $\omega_{\rm phy}$ in both our models.

On the other hand, when qH^* is less than Ξ, δv can go deep down to the small-z region. As the field lines show, δv moves cells from regions with a small tissue thickness to regions with a large tissue thickness; this deviatoric flow slows down the relaxation of the tissue, and this is why $\omega_{\rm phy}|_{q\neq 0}$ is different from $\omega_{\rm phy}|_{q=0}$. When $qH^* \ll 1$, the tissue surface is very flat, therefore this effect due to deviatoric flow is again weak. Therefore $\omega_{\rm phy}|_{q\neq 0}$ is significantly different from $\omega_{\rm phy}|_{q=0}$ when $qH^* \sim \mathcal{O}(1)$.

The last two main results (iv and v) listed at the end of Sec. II B require further discussion. Let us begin with the nonmonotonic behavior of $K^{\rm II}_{\rm phy}$ vs $r_{\rm rel}$. As shown in Figs. 5(a) and 5(b), when $qH^* < \Xi$ as $r_{\rm rel}$ increases, the low-viscosity region increases, and the deviatoric flow from small-H regions to large-H regions becomes stronger; therefore $\omega_{\rm phy}$ is less stabilizing as $r_{\rm rel}$ increases. On the other hand, in Figs. 5(c) and 5(d) one can see that when $qH^* > \Xi$, vortices appear in the deviatoric flow field. Depending on the relative height of h_S and the centers of the vortices, the net flow of cells from low-H regions to high-H regions could increase or decrease as $r_{\rm rel}$ increases. Note that (i) h_S/H^* increases with $r_{\rm rel}$, therefore the green lines in Figs. 5(c) and 5(d) move upward with $r_{\rm rel}$, and (ii) cells below centers of the vortices flow from large-H regions to small-H regions, while cells above centers of the vortices flow from small-H regions to large-H regions. These two facts can help us to understand the dependence of $\omega_{\rm phy}$ on $r_{\rm rel}$. First, in Fig. 5(c) h_S is lower than the centers of the vortices; as $r_{\rm rel}$ increases, more and more cells that flow from large-H regions to small-H regions are in the less viscous region, therefore $\omega_{\rm phy}$ becomes more stabilizing as $r_{\rm rel}$ increases when h_S is lower than the centers of the vortices. On the other hand, Fig. 5(d) shows that when h_S is higher than the centers of the vortices, as $r_{\rm rel}$ increases more cells in the less viscous region move from regions of small H to regions of large H. This is why $\omega_{\rm phy}$ could become less stabilizing as $r_{\rm rel}$ increases when h_S is higher than the centers of the vortices. This explains why the curve with $qH^* = 2(>\Xi)$ in Fig. 2(d) has a nonmonotic dependence of $K^{\rm II}_{\rm phy}$ with respect to $r_{\rm rel}$. It also illustrates the subtle role that deviatoric flow plays in the dynamics of the tissue.

The last main result (v) listed at the end of Sec. II B is that the sign of $K^{\rm II}_{\rm phy}$ can be positive; i.e., it is possible that the overall effect of cell division and apoptosis is to hinder the relaxation of the tissue towards the steady state. The mechanism that drives this effect has already been shown in the flow field, i.e., the deviatoric flow due to cell turnover brings cells in small-H regions to large-H regions. $K^{\rm II}_{\rm phy}$ becomes positive when the following two conditions are both satisfied. (a) The viscosity η_S in the region $h < h_S$ is sufficiently small compared to η_D (the viscosity in the region $z > h_S$). (b) The relative thickness of the proliferative region h_S/H^* is sufficiently large. Note that a tissue that satisfies condition (b) is likely not a normal tissue; as a healthy mature epithelium tissue usually has a relatively thin layer of proliferative cells, a tissue with large h_S/H^* is more likely to be found during development or pathological situations.

To see whether a flat apical surface can become unstable due to a positive $K^{\rm II}_{\rm phy}$, we introduce a dimensionless parameter, $\sigma q/(2\eta_D r_D)$, to describe the relative importance of the apical

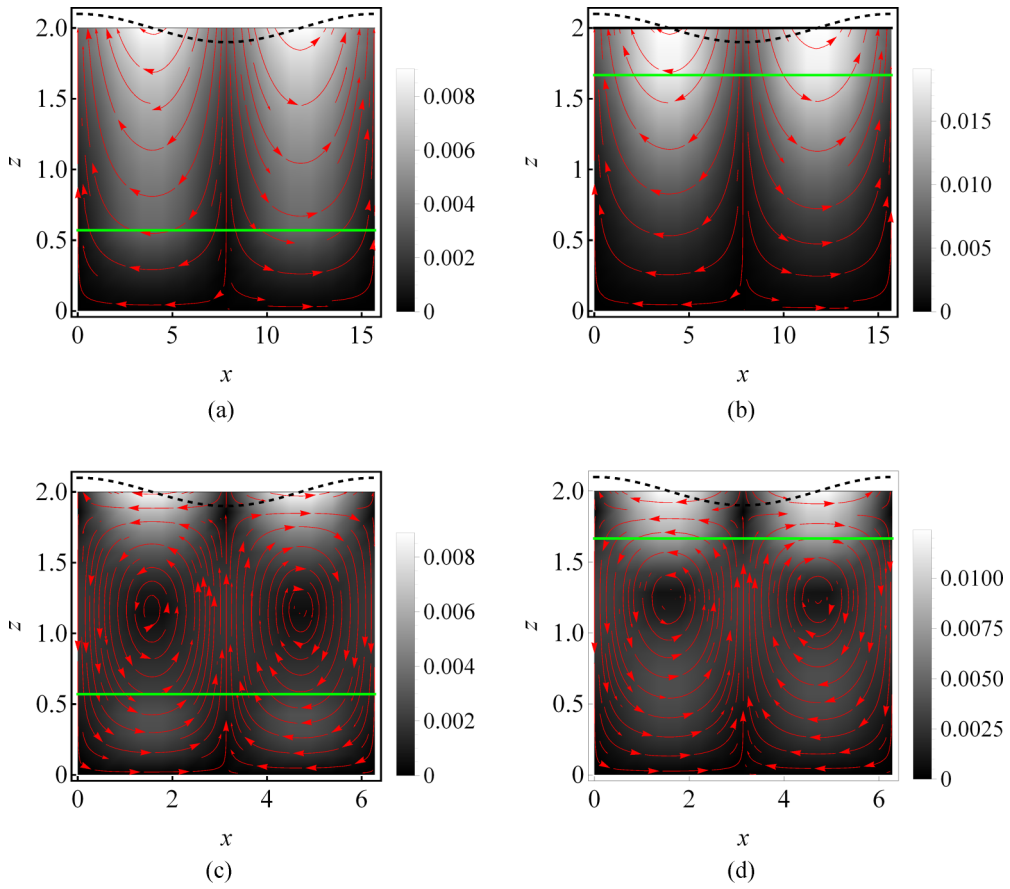

FIG. 5. Field lines of $(\delta v_x, \delta v_y)$ at $t = 0$ in the second model for $\sigma = 0$ for (a) $qH^* = 0.8$ $(qH^* < \Xi)$, $r_{\rm rel} = 0.4$; (b) $qH^* = 0.8$ $(qH^* < \Xi)$, $r_{\rm rel} = 5$; (c) $qH^* = 2.0$ $(qH^* > \Xi)$, $r_{\rm rel} = 0.4$; and (d): $qH^* = 2.0$ $(qH^* > \Xi)$, $r_{\rm rel} = 5$. These field lines describe the δv indicated by the open (a) diamond, (b) square, (c) circle, and (d) triangle in Fig. 2(d). The width along the x axis is chosen to be one wavelength. There are vortices in the deviatoric flow when $qH^* > \Xi$. h_S is indicated by green lines. Flow fields are taken from the solution of the linearized dynamics for $\eta_{\rm rel} = 5$, $k_p(H^*) = -1$, $H^* = 2$, and $\delta H(t = 0) = 0.01\cos(qx)$.

surface tension and cell turnover in tissue dynamics. As shown by comparing Figs. 6(a) and 6(b), tissues with small $\sigma q/(2\eta_D r_D)$ become unstable relatively easily; this is due to the relatively weak stabilizing effect from the apical surface tension. Figure 6(c)–6(f) shows how the growth rate of small perturbations changes with our model parameters. This suggests that increasing r_S and η_S helps to stabilize the steady state, as the peak of the growth rate decreases; on the other hand, increasing r_D and η_D helps to destabilize the steady state, as the maximum growth rate of small perturbations increases. Since h_S/H^* increases (decreases) as r_D (r_S) increases, $\eta_{\rm rel}$ increases (decreases) as η_D (η_S) increases; these results further confirm that a tissue is less stable when $r_{\rm rel}$ and $\eta_{\rm rel}$ become large.

Now we can summarize the role of cell turnover in the dynamics of a tissue close to steady state. Intuitively, when the tissue height is perturbed from its steady-state value, there is an imbalance of cell division events and cell apoptosis events in the tissue, and it drives the tissue toward the steady state. This effect is described by $\omega_{\rm phy}|_{q=0} = k_p(H^*)$. However, at finite q, cell apoptosis on the apical surface induces a deviatoric flow in the tissue that brings cells to thicker regions and pushes cells away from regions of smaller thickness. This deviatoric flow makes $\omega_{\rm phy}|_{qH^*\neq 0}$ less stabilizing than $\omega_{\rm phy}|_{q=0}$. At fixed η_D, this destabilizing effect is more pronounced as the thickness of the proliferative layer increases, as this layer has a lower viscosity, and the effect of deviatoric flow is more significant. For a normal tissue, proliferative cells occupy a small region close to the basal surface; the overall effect of these mechanisms on tissue dynamics always helps to stabilize the tissue. On the other hand, for a tissue with a large proportion of proliferative cells, when the viscosity of the proliferative region of the tissue is sufficiently low compared to the viscosity of the nonproliferative region, the induced flow can destabilize the steady state, and the first instability occurs at wavelength $1/q \sim H^*$.

B. Cell division, cell apoptosis, and tissue viscosity

In Sec. II B we argue that the viscosity in a tissue should depend on the local tissue composition. A derivation of the viscosity from a general hydrodynamic model of stratified epithelium tissue is presented in Appendix B, where we assume that the stress relaxation process receives a negligible contribution from the turnover of junction proteins, and cell division and apoptosis produce a force distribution that dominates the active stress inside a tissue. This approach generalizes the earlier theory of Ranft *et al.* [7] by explicitly

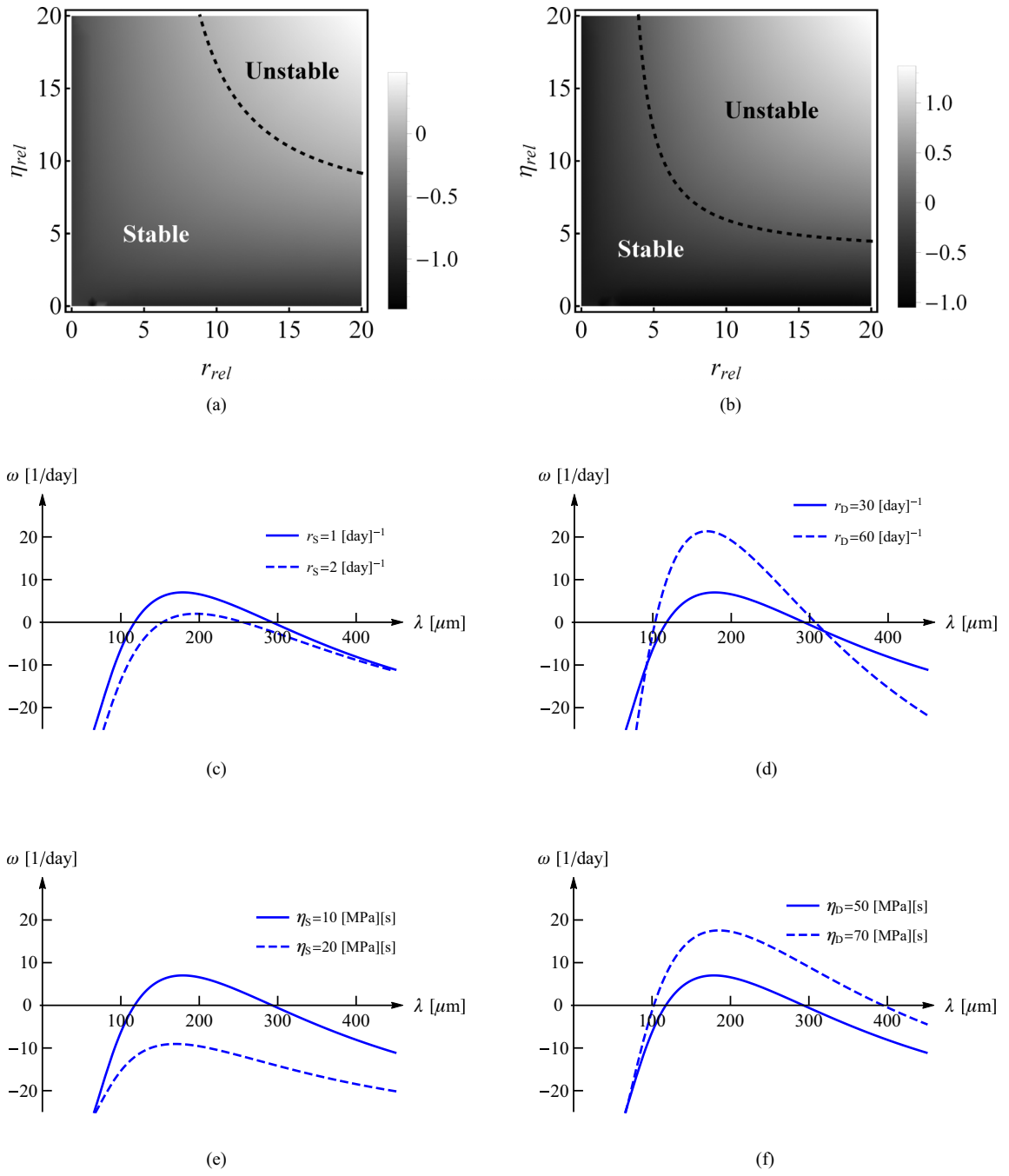

FIG. 6. (a, b) Gray scale indicates the growth rate of a perturbation scaled by r_D for $qH^* = \Xi$: $\sigma q/(2\eta_D r_D) = 0.4$ (a) and $\sigma q/(2\eta_D r_D) = 0.05$ (b). (c–f) Growth rate [in units of 1/day (d^{-1})] of a tissue as a function of the wavelength of perturbation. Solid curves: $r_S = 1\ d^{-1}$, $r_D = 30\ d^{-1}$, $\eta_S = 10$ MPa s, $\eta_D = 50$ MPa s, $\sigma = 1$ m Nm^{-1}. Dashed lines give the relaxation rate versus λ for the same parameters except $r_S = 2\ d^{-1}$ in (c), $r_D = 60\ d^{-1}$ in (d), $\eta_S = 20$ MPa s in (e), and $\eta_D = 70$ MPa s in (f). For (c): dashed curve, $H^* = 32\ \mu$m, $h_S = 30\ \mu$m; solid curve, $H^* = 31\ \mu$m, $h_S = 30\ \mu$m. For (d): dashed curve, $H^* = 30.5\ \mu$m and $h_S = 30\ \mu$m; solid curve, $H^* = 31\ \mu$m and $h_S = 30\ \mu$m. For (e) and (f): all curves, $H^* = 31\ \mu$m and $h_S = 30\ \mu$m.

including the contribution from different types of cells in a tissue [34,36]. From Eqs. (B17) and (B18), the viscosity η in a tissue can be expressed as

$$\eta = \frac{\mu\sigma_0}{\rho_S r_S d_S + \rho_D r_D \tilde{d}_D}, \tag{18}$$

where ρ_S is the number density of proliferative cells and ρ_D is the number density of nonproliferative cells. μ is the shear modulus of the tissue, r_S is the cell division rate, and r_D is the cell apoptosis rate. When a cell divides, it acts as a force dipole with a direction given by the cell division mitotic axis. The strength of this force dipole is described by d_S, and this force dipole gives a stress that contributes to the tissue dynamics under shear. When a cell undergoes apoptosis, its neighboring cells produce a contraction that tends to fill the void left by the dead cell. If the tissue is locally anisotropic, this contraction

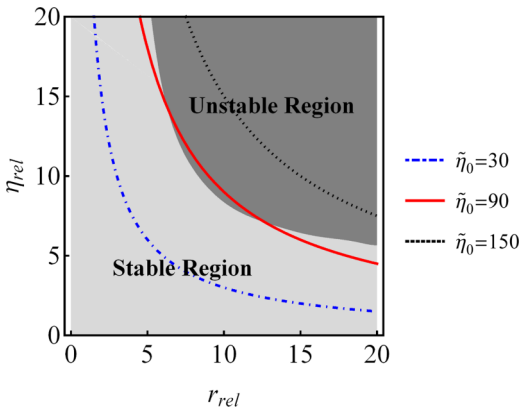

FIG. 7. $r_{\rm rel}$ versus $\eta_{\rm rel}$ [from Eq. (18)] for $\tilde{\eta}_0 = 30$ (blue curve), $\tilde{\eta}_0 = 90$ (red curve), and $\tilde{\eta}_0 = 150$ (yellow curve). The short-dashed curve is the stability boundary for a tissue with $\sigma q/(2\eta_D r_D) = 0.2$ and $qH^* = \Xi$. For the dark-gray region, $\omega|_{qH^*=\Xi} > 0$; for the light-gray region, $\omega|_{qH^*=\Xi} < 0$

produces a shear stress that contributes to the shear viscosity of the tissue. $\tilde{d}_D$ characterizes the strength of the stress induced by this anisotropy. σ_0 is a characteristic stress that describes the response of cell polarity to the stress in a tissue: cells in a tissue with a smaller σ_0 are more likely to be polarized by mechanical stress. Indeed, Eq. (18) shows that viscosity in a tissue depends on the local proportion of proliferative cells.

In our second model all the proliferative cells are localized in the basal ($z < h_S$) region, $\rho_S = \rho$ for $z < h_S$ and $\rho_S = 0$ for $z > h_S$. From Eq. (18), the viscosity in the tissue can be expressed as

$$\eta(z) = \begin{cases} \frac{\mu\sigma_0}{\rho r_S d_S} = \eta_S, & z < h_S; \\ \frac{\mu\sigma_0}{\rho r_D \tilde{d}_D} = \eta_D, & z > h_S. \end{cases} \tag{19}$$

From Eq. (19), it is clear that the relative viscosity $\eta_{\rm rel} \equiv \eta_D/\eta_S$ and the relative proliferative rate $r_{\rm rel} \equiv r_D/r_S$ are not independent. In fact one can express $\eta_{\rm rel}$ as

$$\eta_{\rm rel} = \frac{\tilde{\eta}_0}{r_{\rm rel}}, \tag{20}$$

where $\tilde{\eta}_0 \equiv d_S/\tilde{d}_D > 0$ is a dimensionless parameter.

Equation (20) indicates that, for a given $\tilde{\eta}_0$, a tissue has a large $\eta_{\rm rel}$ when the magnitude of $r_{\rm rel}$ is small. A normal tissue has a relatively thin proliferative region, i.e., small $r_{\rm rel}$, therefore as long as $\tilde{\eta}_0$ is of order unity, it has $\eta_{\rm rel} > 1$. However, a normal tissue is likely to have a stable steady state because its $r_{\rm rel}$ is small.

To see when the steady state becomes unstable, Fig. 7 shows $\eta_{\rm rel}$ versus $r_{\rm rel}$ for a few choices of $\tilde{\eta}_0$ and the stability boundary of an epithelium tissue described by our second model. It is clear that for the contribution from $\omega_{\rm phy}$ to drive the tissue to instability, the magnitude of $\tilde{\eta}_0$ has to be large [$\sim\mathcal{O}(100)$]. Thus we predict that a tissue with a small $\tilde{d}_D$ is more likely to have a nonflat homeostasis state.

Although we show in Appendix B that it is possible to estimate $\tilde{d}_D$ from experiments, so far we have not found any estimate of both d_S and $\tilde{d}_D$ from the same tissue. Thus we can only state that, in principle, different tissues may have very different $\tilde{\eta}_0$'s. Even for the same tissue, a mutation can change $\tilde{d}_D$ to make $\tilde{\eta}_0$ greater than its normal magnitude. This could eventually drive a flat apical surface toward instability. Since this article reports a theoretical prediction, future experiments will be important to determine the value of $\tilde{\eta}_0$ in real wild-type tissues and tissues with mutations, as it is an important link between cellular property and tissue mechanics.

Note that the viscosity shown in Eq. (18) is derived for a tissue whose cell adhesion protein turnover makes a negligible contribution to its viscosity. For a tissue in which the proliferative cells have a small number of intercellular adhesion sites compared to TD cells, $\eta_{\rm rel}$ could be greater than the magnitude predicted by Eq. (20). Therefore when both turnover of cell adhesion proteins and active force dipoles due to cell division or cell apoptosis contribute significantly to tissue dynamics, one still should treat $r_{\rm rel}$ and $\eta_{\rm rel}$ as independent parameters.

IV. CONCLUSION

Although biological tissues exhibit a high plasticity that allows remodeling, the homeostasis state is regulated such that its architecture is robust against intrinsic fluctuations and external perturbations [2,36]. In this article we have studied how the local tissue composition affects its viscous properties, and how the viscous properties in turn affect the dynamics of a tissue close to the steady state of a stratified epithelium. In a tissue with proliferative cells located close to the basal membrane and differentiated cells located close to the apical surface, the lower region of the tissue has a different viscosity compared to the upper region. Since cell division or apoptosis inevitably induces a flow in this tissue, the position-dependent viscosity in the tissue has a profound effect on its dynamics.

Our analysis shows that although cell division and cell apoptosis in a tissue are regulated to maintain the tissue steady state, when the thickness of a tissue is perturbed by a nonzero q height modulation there is a flow induced by cell turnover that brings cells from small thickness regions to large thickness regions. This flow hinders the relaxation towards the steady state. We find that perturbations with wavelengths comparable to the thickness of the tissue have the slowest relaxation rate toward the steady state. When the tissue has a thick proliferative region, and the viscosity of the proliferative region is significantly smaller than the other region, the steady state can even become unstable. We also calculate the relation between tissue viscosity and tissue composition and active forces that is generated during cell division and cell apoptosis. From our analysis, we find a link between the key parameters $\eta_{\rm rel}$ and $r_{\rm rel}$ of tissue dynamics and the force dipoles during cell division and cell apoptosis. This link suggests a possible change of cellular properties that can lead to the instability of a flat tissue.

It is important to note that our analysis suggests a different tissue instability from the proposals in previous models [33–35]. First, although the apical surface was also perturbed, in these studies the focus was the instability of the tissue-stroma interface; this is different from our model, where we assume a rigid stroma and the dynamics of the apical surface is the focus. Furthermore, in these previous studies the viscosity in the tissue is homogeneous, but in our model the instability only

occurs when the viscosity difference between the proliferative region and the nonproliferative region is sufficiently large.

Our model is quite general, thus our prediction should hold in general for stratified continuous self-renewal tissues. In the context of stratified epithelium, many undulating patterns, for example, rete peg [23–25], occur at the basal lamina, and its mechanical origin has been explained by previous theoretical works [29,33–35]. On the other hand, our result provides a possible route to trigger epithelial apical surface undulations. Although instability due to the induced flow described by our model is unlikely to happen in a stratified tissue with a thin layer of proliferative cells, this mechanism could be important during embryogenesis and tumor growth because of the presence of a relatively large proportion of proliferative cells. Furthermore, when two tissues are in contact [12], the viscosity difference between these two tissues could also lead to interesting hydrodynamic instabilities. These possibilities will be explored in our future work. It is also worth mentioning that although, in principle, apical surface patterns can be the result of an inhomogeneous distribution of growth factors in the tissue [34], our model reveals that it could also be induced purely by mechanical forces distributed in the tissue [33–35].

To test our theory in *in vitro* experiments, one could try to increase $r_{\rm rel}$ by increasing the apoptosis rate of differentiated cells or try to decrease the tissue apical surface tension to make the contribution from $\omega_{\rm phy}$ relatively more significant. In the case of mammalian olfactory epithelium, a higher apoptosis rate can be induced by unilateral olfactory bulbectomy [39]. The apical surface tension originates from cell-cell adhesion and active tension of the cell cortex [1,2,40], and it could be decreased by, for example, the protease digestion procedure [41].

Several modifications can be made to make our model more general. For example, the solid stroma in our model can be easily replaced by a soft stroma [33–35]. The assumption that the thickness of the proliferative region h_S is a constant can be relaxed if we include the dynamics of some small molecules which can trigger cell differentiation in the model [36]. Another important improvement that we will make in future work is to develop a model in which the cell distribution is not predefined. It is important to check how homeostasis state and pattern formation are achieved in a stratified epithelium with a more general hydrodynamic model. The dynamics of cell lineage [34,42,43] will have to be taken into account in this future work.

ACKNOWLEDGMENTS

The authors would like to thank the Ministry of Science and Technology, Taiwan (Grant No. 102-2112-M-008-008-MY3), and NCTS for support. The authors are also grateful for stimulating discussions with J.-F. Joanny (ESPCI) and helpful discussions with C.-M. Chen (National Yang-Ming University, Taiwan).

APPENDIX A: DERIVATION OF THE GROWTH RATE OF A PERTURBATION

In this Appendix, we present the derivation of the growth rate of a small perturbation of the tissue height. We first discuss the calculation in our first model, in which the tissue has a constant viscosity, then explain how to use a similar method to calculate the growth rate for our second model, where the viscosity takes different values in the region occupied by proliferative cells and the rest of the tissue.

1. First model

Equations (6) and (7) describe the linearized dynamics of the tissue. The deviatoric velocity field satisfies the no-slip condition at $z = 0$, i.e.,

$$\delta v_x|_{z=0} = \delta v_z|_{z=0} = 0, \tag{A1}$$

and the linearized stress-balance condition at the apical surface, i.e., Eqs. (8) and (9). The evolution of the apical surface is described by the linearized kinematic boundary condition, Eq. (10). Equations (6) and (7) indicate that the deviatoric flow inside the tissue is not driven by any active processes, but the contribution from $k_p(H^*)$ in the shear stress continuity equation at the apical surface, Eq. (9), indicates that for a tissue under perturbation, there is a driving force acting on the apical surface that originates from cell apoptosis.

Note that although there are three variables, δv_x, δv_z, and δp, in the force balance equation, Eq. (7), the constraint given by Eq. (6) tells us that there are only two independent variables. Since Eq. (7) actually contains two second-order differential equations, we should have four independent solutions, and the general solution is a linear combination of these four independent solutions with coefficients determined by the four boundary conditions, Eq. (A1), Eq. (8), and Eq. (9).

Consider a perturbation of the tissue height H that can be expressed as $\delta H(x,t) = \hat{H}\exp(\omega t + iqx)$, where q is the wave number of the perturbation. The deviatoric flow and pressure induced by this perturbation are

$$\begin{pmatrix} \delta v_x(x,z,t) \\ \delta v_z(x,z,t) \\ \delta p(x,z,t) \end{pmatrix} = \begin{pmatrix} \hat{v}_x \\ \hat{v}_z \\ \hat{p} \end{pmatrix} e^{\omega t + iqx + kz}. \tag{A2}$$

Here $\hat{v}_x$, $\hat{v}_z$, $\hat{p}$, and $\hat{H}$ are constants. Note that in general ω and k are complex. Substituting Eq. (A2) into Eq. (6) and Eq. (7), we obtain a matrix equation:

$$\begin{pmatrix} iq & k & 0 \\ \eta(k^2-q^2) & 0 & -iq \\ 0 & \eta(k^2-q^2) & -k \end{pmatrix} \begin{pmatrix} \hat{v}_x \\ \hat{v}_z \\ \hat{p} \end{pmatrix} = \begin{pmatrix} 0 \\ 0 \\ 0 \end{pmatrix}. \tag{A3}$$

The condition for Eq. (A3) to have a nontrivial solution is $k = \pm q$. It is then easy to find the following two solutions for Eq. (6) and Eq. (7) from the eigenvectors of the matrix in Eq. (A3):

$$\psi_1 = \begin{pmatrix} 1 \\ i \\ 0 \end{pmatrix} e^{\omega t + iqx - qz}, \quad \psi_2 = \begin{pmatrix} 1 \\ -i \\ 0 \end{pmatrix} e^{\omega t + iqx + qz}. \tag{A4}$$

To find the other two solutions, we look for solutions of the following form

$$\begin{pmatrix} \delta v_x(x,z,t) \\ \delta v_z(x,z,t) \\ \delta p(x,z,t) \end{pmatrix} = \left[\begin{pmatrix} \zeta_1 \\ \zeta_2 \\ \zeta_3 \end{pmatrix} + z \begin{pmatrix} \zeta_4 \\ \zeta_5 \\ \zeta_6 \end{pmatrix} \right] e^{\omega t + iqx \pm qz}; \tag{A5}$$

here ζ_i's are constants. Substituting the above ansatz into Eq. (6) and Eq. (7) and solving ζ_i's, we obtain two more solutions:

$$\psi_3 = \left[\begin{pmatrix} -1 \\ -1/q - i \\ -2\eta \end{pmatrix} + iz \begin{pmatrix} 1 \\ i \\ 0 \end{pmatrix} \right] e^{\omega t + iqx - qz} \tag{A6}$$

and

$$\psi_4 = \left[\begin{pmatrix} 1 \\ -1/q - i \\ 2\eta \end{pmatrix} + iz \begin{pmatrix} 1 \\ -i \\ 0 \end{pmatrix} \right] e^{\omega t + iqx + qz}. \tag{A7}$$

The physical solution of the deviatoric flow and pressure fields is a linear combination of ψ_1, ψ_2, ψ_3, and ψ_4. From the four boundary conditions, Eq. (A1) and Eqs. (8) and (9), these coefficients can be found. Substituting the solution for the deviatoric flow and pressure into the kinematic boundary condition, Eq. (10), one obtains the dispersion relation, Eq. (11), with ω_{mech} and ω_{phy} given in Eq. (12) and Eq. (13).

2. Second model

Now we explain how to derive the dispersion relation for a perturbation in our second model. Besides the four boundary conditions at $z = 0$ and $z = H^*$ that have been described in our first model, because the viscosity difference between the $z < h_S$ region and the $z > h_S$ region, there are four continuous conditions for the flow field, normal stress, and shear stress at $z = h_S$,

$$\begin{aligned} \lim_{z \to h_S^-} v_i &= \lim_{z \to h_S^+} v_i, \\ \lim_{z \to h_S^-} \sigma_{zi} &= \lim_{z \to h_S^+} \sigma_{zi}, \end{aligned} \tag{A8}$$

where $i = x, z$.

The deviatoric flow field and pressure at $0 < z < h_S$ and $h_S < z < H^*$ satisfy the same equations, Eq. (6) and Eq. (7), with $\eta = \eta_S$ for $z < h_S$ and $\eta = \eta_D$ for $z > h_S$. This is similar to our first model, but now we have two matrix equations to solve, and there are four independent solutions for each matrix equation. The physical solution in each region is a linear combination of the four solutions of its corresponding matrix equation. Then the eight boundary conditions, Eq. (8), Eq. (9), Eq. (A1), and Eq. (A8), are applied to determine all these coefficients. The dispersion relation for the tissue surface can then be obtained from the kinematic boundary condition, Eq. (9). After tedious but straightforward calculations we find that ω can still be expressed as the sum of two terms; one term (denoted ω_{mech}) is expressed by Eq. (16), and the other term (denoted ω_{phy}) is expressed by Eq. (17), where $K^{\text{II}}_{\text{mech}}$ and $K^{\text{II}}_{\text{phy}}$ are

$$K^{\text{II}}_{\text{mech}} = \frac{(\eta_{\text{rel}}+1)^2(2qH^* - \sinh qH^*) + (\eta_{\text{rel}} - 1)^2\mu_1}{(\eta_{\text{rel}}+1)^2[1+2(qH^*)^2 + \cosh 2qH^*) + (\eta_{\text{rel}} - 1]^2\mu_2} \tag{A9}$$

and

$$K^{\text{II}}_{\text{phy}} = \frac{-(\eta_{\text{rel}} + 1)^2(1 + \cosh 2qH^*) + (\eta_{\text{rel}} - 1)^2(\mu_3 - \mu_2)}{(\eta_{\text{rel}} + 1)^2[1 + 2(qH^*)^2 + \cosh 2qH^*] + (\eta_{\text{rel}} - 1)^2\mu_2.} \tag{A10}$$

Here the μ_i's depend on qH^* and $\tilde{h}_S$ ($\tilde{h}_S \equiv h_S/H^*$); they are

$$\begin{aligned} \mu_1 \equiv\ & 2qH^*\{1 - 2\tilde{h}_S[1 + 2(qH^*)^2](\tilde{h}_S - 1)\tilde{h}_S\} + 4qH^*(\tilde{h}_S - 1)\cosh(2qH^*\tilde{h}_S) - \sinh[2qH^*(1 - 2\tilde{h}_S)] \\ & + 2\left[1 + 2(qH^*)^2\tilde{h}_S^2\right]\sinh[2qH^*(1 - \tilde{h}_S)], \end{aligned} \tag{A11}$$

$$\begin{aligned} \mu_2 \equiv\ & 1 + 2(qH^*)^2\{1 + 4(\tilde{h}_S - 1)\tilde{h}_S[1 + (qH^*)^2(\tilde{h}_S - 1)\tilde{h}_S]\} + \cosh[2qH^*(1 - 2\tilde{h}_S)] \\ & - 2\left[1 + 2(qH^*)^2\tilde{h}_S^2\right]\cosh[2qH^*(\tilde{h}_S - 1)] - 2[1 + 2(qH^*)^2(\tilde{h}_S - 1)^2]\cosh(2qH^*\tilde{h}_S), \end{aligned} \tag{A12}$$

and

$$\mu_3 \equiv 2(qH^*)^2\{1 + 2\tilde{h}_S[-2 + (1 + 2(qH^*)^2(\tilde{h}_S - 1)^2)\tilde{h}_S]\} + 2(\tilde{h}_S - 1)^2\cosh(2qH^*\tilde{h}_S). \tag{A13}$$

Note that, as pointed out in Sec. III, $K^{\text{II}}_{\text{mech}} \to -1$ as $qH^* \to \infty$, and $K^{\text{II}}_{\text{phy}} \to -1$ as $qH^* \to \infty$ or $qH^* \to 0$.

APPENDIX B: VISCOSITY IN A TISSUE

In this Appendix we first construct a general model for continuous self-renewing tissues that includes both spatial and cell lineage dynamics. By assuming that cell division and apoptosis dominate the stress relaxation in a tissue, we show that a tissue behaves as a viscoelastic material, and the viscosity in a tissue depends on the local tissue composition. The parameters in the theory can be measured with existing experimental methods. The analysis in this Appendix follows closely the work of Ranft *et al.* [7]. The main difference is that in our model the cell lineage, which has been identified as the fundamental unit of tissue and organ development [36], is also taken into account.

There are proliferative cells and terminally differentiated cells in a tissue. Typically, proliferative cells include stem cells and transit-amplifying cells differentiated from stem cells. For simplicity, we ignore this internal conversion of proliferative cells and note only that proliferative cells can undergo cell division, and the daughter cells have a certain chance of becoming TD cells. On the other hand, TD cells do not divide; they only undergo programmed cell death (apoptosis). Similarly to other models [34,36,42], ours neglect apoptosis of proliferative cells.

Because of the coupling between the cortical network and the adhesion proteins, cells in a tissue are tightly connected [2,5], and diffusion of cells inside the tissue can be neglected [44]. Denote ρ_S the number density of proliferative cells and ρ_D the number density of TD cells. Taking into account cell division and apoptosis, and advection of cells by the flow inside the tissue, the continuity equations for ρ_S and ρ_D can be written as

$$\partial_t \rho_S + \partial_l(v_l \rho_S) = r_S(2p_S - 1)\rho_S, \tag{B1}$$

$$\partial_t \rho_D + \partial_l(v_l \rho_D) = 2r_S(1 - p_S)\rho_S - r_D \rho_D, \tag{B2}$$

where the Einstein summation convention is used to simplify the notation, and r_S and r_D are the division rate of proliferative cells and the apoptosis rate of TD cells, respectively. p_S is the self-renewal probability of proliferative cells, and v_i ($i = x,y,z$) is the ith component of the flow field.

The total cell density at position $\mathbf{r}$ is $\rho(\mathbf{r},t) = \rho_S(\mathbf{r},t) + \rho_D(\mathbf{r},t)$. The fraction of the proliferative cells at $\mathbf{r}$ is $\Lambda_S(\mathbf{r},t) = \rho_S(\mathbf{r},t)/\rho(\mathbf{r},t)$. From Eqs. (B1) and (B2), the evolution equations for ρ and Λ_S are

$$D_t \rho = \rho[(r_S + r_D)\Lambda_S - r_D - \partial_l v_l], \tag{B3}$$

$$D_t \Lambda_S = [2r_S p_S - r_S + r_D - (r_S + r_D)\Lambda_S]\Lambda_S, \tag{B4}$$

where $D_t \equiv \partial_t + v_l \partial_l$ is the material derivative.

We assume that, in the absence of active processes such as cell division and cell apoptosis, a tissue behaves as a linear elastic material, thus there is a linear relation between the change of elastic stress $\Delta\sigma^E_{ik}$ and the change of elastic strain Δu_{ik}, $\Delta\sigma^E_{ik} = (K - 2\mu/3)\Delta u_{ll}\delta_{ik} + 2\mu\Delta u_{ik}$, where K is the compressional modulus and μ is the shear modulus [45]. Besides elastic stress, cell division and cell apoptosis also exert forces to the tissue [46]. Because these processes exert no net force and torque on the tissue [47,48], we model them as symmetric force dipoles [7,47,49]. For a cell division or apoptosis event occurring at $\mathbf{r} = \mathbf{r}_0$, the change of stress is related to the active force dipole d_{ik} through $\Delta\sigma^A_{ik} = -d_{ik}\delta(\mathbf{r} - \mathbf{r}_0)$, where $\delta(\mathbf{r} - \mathbf{r}_0)$ is the Dirac delta function and the superscript A denotes stress created by active cell division or apoptosis events. Since the inertia is negligible [50], the force balance condition gives

$$\partial_i \sigma_{ik} = 0, \tag{B5}$$

where $\sigma_{ik} \equiv \sigma^E_{ik} + \sigma^A_{ik}$ is the total stress in the tissue.

Due to cell division and apoptosis, a unique reference state for the strain does not exist. However, the difference in strain between subsequent states still can be defined [7]. Letting the frame of reference flow and rotate with the local flow and vortex, the evolution equation for the stress can be written as

$$D^J_t \sigma_{ik} = \left(K - \tfrac{2}{3}\mu\right)v_{ll}\delta_{ik} + 2\mu v_{ik} + D^J_t \sigma^A_{ik}, \tag{B6}$$

where $D^J_t \sigma_{ik} \equiv D_t \sigma_{ik} + \Omega_{il}\sigma_{lk} + \Omega_{kl}\sigma_{il}$ is the Jaumann derivative. Here $v_{ik} \equiv (\partial_i v_k + \partial_k v_i)/2$ is the strain rate tensor, and $\Omega_{ik} \equiv (\partial_i v_k - \partial_k v_i)/2$ is the vorticity tensor.

It is convenient to decompose the total stress tensor into isotropic and traceless parts, i.e., $\sigma_{ik} = -p\delta_{ik} + \tilde{\sigma}_{ik}$, where $p \equiv -\sigma_{ll}/3$ is the tissue pressure and $\tilde{\sigma}_{ik}$ is the traceless (deviator) part of the total stress tensor. Physically the isotropic part of the stress tensor is related to the change in the local tissue volume, and $\tilde{\sigma}_{ik}$ is related to the distortion of the local tissue shape [45]. The same decomposition can also be applied to the active stress tensor and strain rate tensor, i.e., $\sigma^A_{ik} = -p^A\delta_{ik} + \tilde{\sigma}^A_{ik}$ and $v_{ik} = (1/3)v_{ll}\delta_{ik} + \tilde{v}_{ik}$. Now the stress evolution, Eq. (B6), can be expressed as

$$D_t p = -K v_{ll} + D_t p^A \tag{B7}$$

and

$$D^J_t \tilde{\sigma}_{ik} = 2\mu\tilde{v}_{ik} + D^J_t \tilde{\sigma}^A_{ik}. \tag{B8}$$

To complete our model, we still need the constitutive equations for $D_t p^A$ and $D^J_t \tilde{\sigma}^A_{ik}$. Active stress is induced by cell division and cell apoptosis; we first consider the force dipole created by cell division. Let the unit vector $\hat{l}_i$ denote the direction of the cell division mitotic axis (Fig. 8); following [51], the force dipole produced by a cell division event can be approximated by

$$d^{\text{div}}_{ik} = 3d_S\hat{l}_i\hat{l}_k. \tag{B9}$$

Here d_S characterizes the strength of the dipole. Typically $d_S > 0$ because cell division makes tissue grow. Since different dividing cells may have different mitotic axes, the macroscopic property is related to the average of d_{ik} in a small region,

$$\left\langle d^{\text{div}}_{ik}\right\rangle = 3d_S\langle\hat{l}_i\hat{l}_k\rangle = d_S(\delta_{ik} + \tilde{q}_{ik}), \tag{B10}$$

where $\tilde{q}_{ik} \equiv \langle 3\hat{l}_i\hat{l}_k - \delta_{ik}\rangle$ is the nematic order tensor in the liquid crystal literature. In general, tissue growth and cell division or apoptosis processes are intrinsically anisotropic [5,7,52–54], and the orientation of the cell mitotic axis depends on local tissue distortion [7,55,56]. To linear order, this relation can be expressed as

$$\tilde{q}_{ik} - \tilde{q}^0_{ik} = \frac{\tilde{\sigma}_{ik}}{\sigma_0}, \tag{B11}$$

where $\sigma_0 > 0$ is a constant and $\tilde{q}^0_{ik}$ is the intrinsic anisotropic tensor, which should satisfy $\tilde{q}^0_{ll} = 0$. Denoting the eigenvalues of $\tilde{q}_{ik} - \tilde{q}^0_{ik}$ as $\tilde{q}^{(i)}$, it is convenient to write

$$\tilde{q}^{(i)} = 3\langle\cos^2\theta_i\rangle - 1, \tag{B12}$$

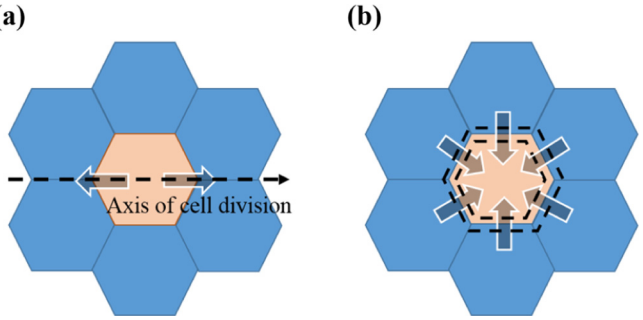

FIG. 8. Cell division and apoptosis as a source of localized force inside tissue. (a) Cell division produces equal but opposite forces along the mitotic axis (dashed arrow). (b) Cell apoptosis induces a purse string (dashed line) which shrinks the cell surface and prevents gap formation. Both processes create a force dipole acting on the surrounding environment (blue cells).

where θ_i is the direction angle of the mitotic axis relative to the ith principle axis of $\tilde{q}_{ik} - \tilde{q}^0_{ik}$. From Eq. (B11) we have

$$S_i = \frac{1}{6\sigma_0}\left(3\sigma^{(i)} - \sum_{k=1}^{3}\sigma^{(k)}\right), \tag{B13}$$

where $S_i \equiv (3\langle\cos^2\theta_i\rangle - 1)/2$ is the three-dimensional order parameter relative to the ith principal axis of $\tilde{q}_{ik} - \tilde{q}^0_{ik}$, and $\sigma^{(i)}$'s are the ith eigenvalues of σ_{ik}. From this relation, one can estimate σ_0 from experimental measurements [56].

Cell apoptosis, a key mechanism of tissue morphogenesis [57,58], also exerts force on the surrounding environment (Fig. 8). During apoptosis, a cell rapidly develops an actomyosin ring around its periphery and signals to neighboring cells to induce a "purse-string"-like contractility in the neighboring cells [59]. This purse-string contraction depends on myosin activity, which can be elevated by applying mechanical forces to the tissues [60]. Therefore, in general the force dipole exerted by cell apoptosis is anisotropic and dependent on the local stress,

$$\left\langle d^{\text{apo}}_{ik}\right\rangle = d_D\delta_{ik} + \tilde{d}_D\left(\tilde{q}^0_{ik} + \frac{\tilde{\sigma}_{ik}}{\sigma_0}\right); \tag{B14}$$

the traceless part of this force dipole has an intrinsic contribution proportional to $\tilde{q}^0_{ik}$ and a contribution induced by local stress. d_D and $\tilde{d}_D$ are constants characterizing the strength of the isotropic and the traceless part of the dipole. Typically $d_D < 0$ since cell apoptosis often leads to a decrease in the tissue volume. On the other hand, there is no simple intuitive argument to determine the the sign of $\tilde{d}_D$.

Substitute Eqs. (B10) and (B14) into Eqs. (B7) and (B8) leads to

$$D_t p = -K v_{ll} + \rho[(r_S d_S - r_D d_D)\Lambda_S + r_D d_D], \tag{B15}$$

$$\left(1 + \tau D^J_t\right)\tilde{\sigma}_{ik} = 2\eta\tilde{v}_{ik} + \tilde{\sigma}^I_{ik}, \tag{B16}$$

where $\tilde{\sigma}^I_{ik} \equiv \tau\rho[(r_S d_S - r_D\tilde{d}_D)\Lambda_S + r_D\tilde{d}_D]\tilde{q}^0_{ik}$ is the intrinsic active stress due to the cell's intrinsic polarity, and the time scale τ that characterizes the active stress induced by cell proliferation or apoptosis is

$$\tau \equiv \frac{\sigma_0}{\rho[(r_S d_S - r_D\tilde{d}_D)\Lambda_S + r_D\tilde{d}_D]}, \tag{B17}$$

the viscosity of the tissue is simply

$$\eta = \tau\mu. \tag{B18}$$

From Eq. (B16) and Eq. (B17), we make the following remarks.

(i) For a tissue with no intrinsic cell polarity, $\tilde{\sigma}^I_{ik} = 0$. The stress evolution, Eq. (B16), reduces to the Maxwell model of a viscoelastic material with stress relaxation time τ and viscosity η. At a time scale greater than τ, the tissue behaves like a fluid [61]:

$$\tilde{\sigma}_{ik} = 2\eta\tilde{v}_{ik}. \tag{B19}$$

It is important to note that η depends on ρ and Λ_S. This supports the intuitive argument presented in the text: that the tissue viscosity depends on the local density of proliferative cells and TD cells.

(ii) From Eq. (B17), a sufficient condition for the tissue viscosity to be positive is $\tilde{d}_D > 0$. This is consistent with what has been observed in experiments [8–10].

(iii) In general, $\tilde{\sigma}^I_{ik}$ is not 0. In this case, in the long-time limit the stress of the tissue satisfies

$$\tilde{\sigma}_{ik} = 2\eta\tilde{v}_{ik} + \tilde{\sigma}^I_{ik}. \tag{B20}$$

The additional term on the right-hand side of the above equation suggests that a tissue in a flow-free state is, in general, under stress. This is the active stress from cells with intrinsic polarity. It is important for tissue morphogenesis, for example, in the imaginal disc of *Drosophila* [7,54].

At a time scale large compared to τ, the total stress tensor in a tissue reduces to

$$\sigma_{ik} = -p\delta_{ik} + 2\eta\tilde{v}_{ik} + \tilde{\sigma}^I_{ik}. \tag{B21}$$

Hence a tissue in this limit behaves as a viscous fluid coupled to a scalar field Λ_S and an order parameter which measures the intrinsic anisotropy of cell orientation. Moreover, Eq. (B21), Eqs. (B3)–(B5), and Eq. (B15) give a close set of equations describing tissue and cell lineage dynamics. Note that the constitutive relation we use in the text describes a tissue with negligible intrinsic active stress.

Existing experimental techniques can measure the cell-scale parameters in the hydrodynamics formulation discussed in this Appendix. For example, d_S in Eq. (B9) can be measured by monitoring the traction stress exerted in dividing cells on a flexible substrate [51]. σ_0 can be obtained by measuring the average cell division orientation as a function of the local strain rate. This has been performed for a monolayer of cells [56]. The apoptosis rate, r_D, in a tissue has been measured for the dorsal closure process of *Drosophila* [57]. Furthermore, experimental techniques for measuring the relaxation time τ and the ratio of proliferative cells Λ_S have been reported before [62]. Supposing that all these measurement can be performed on the same tissue, then from Eq. (B17), the magnitude of $\tilde{d}_D$ can be obtained.

In summary, in this Appendix we have presented a theoretical model to relate the viscosity of a tissue to a few measurable parameters. The key parameters, d_S, $\tilde{d}_D$, and σ_0, of a tissue can be measured from different experiments. Therefore it is possible to infer the hydrodynamic properties of a tissue using existing experimental techniques.

[1] D. Gonzalez-Rodriguez, K. Guevorkian, S. Douezan, and F. Brochard-Wyart, Soft matter models of developing tissues and tumors, Science **338**, 910 (2012).

[2] T. Lecuit and P. F. Lenne, Cell surface mechanics and the control of cell shape, tissue patterns and morphogenesis, Nat. Rev. Mol. Cell Biol. **8**, 633 (2007).

[3] M. C. Marchetti, J.-F. Joanny, S. Ramaswamy, T. B. Liverpool, J. Prost, M. Rao, and R. A. Simha, Hydrodynamics of soft active matter, Rev. Mod. Phys. **85**, 1143 (2013).
[4] S. Yang, K. Khare, and P. C. Lin, Harnessing surface wrinkle patterns in soft matter, Adv. Funct. Mater. **20**, 2550 (2010).
[5] M. Perez-Moreno, C. Jamora, and E. Fuchs, Sticky business: Orchestrating cellular signals at adherens junctions, Cell **112**, 535 (2003).
[6] O. Thoumine, M. Lambert, R. M. Mege, and D. Choquet, Regulation of *n*-cadherin dynamics at neuronal contacts by ligand binding and cytoskeletal coupling, Mol. Biol. Cell **17**, 862 (2006).
[7] J. Ranft, M. Basan, J. Elgeti, J.-F. Joanny, J. Prost, and F. Julicher, Fluidization of tissues by cell division and apoptosis, Proc. Natl. Acad. Sci. U.S.A. **107**, 20863 (2010).
[8] I. Bonnet, P. Marcq, F. Bosveld, L. Felter, Y. Bellaiche, and F. Graner, Mechanical state, material properties and continuous description of an epithelial tissue, J. R. Soc. Int. **9**, 2614 (2012).
[9] R. A. Foty, G. Forgacs, C. Pfleger, and M. S. Steinberg, Liquid Properties of Embryonic Tissues: Measurement of Interfacial Tensions, Phys. Rev. Lett. **72**, 2298 (1994).
[10] G. Forgacs, R. A. Foty, Y. Shafrir, and M. S. Steinberg, Viscoelastic properties of living embryonic tissues: A quantitative study, Biophys. J. **74**, 2227 (1998).
[11] O. Thoumine and A. Ott, Time scale dependent viscoelastic and contractile regimes in fibrobalsts probed by microplate manipulation, J. Cell Sci. **110**, 2109 (1997).
[12] M. Basan, T. Risler, J.-F. Joanny, X. Sastre-Garau, and J. Prost, Homeostatic competition drives tumor growth and metastasis nucleation, HFSP J. **3**, 265 (2009).
[13] A. Z. Rizvi and M. H. Wong, Epithelial stem cells and their niche: There is no place like home, Stem Cells **23**, 150 (2005).
[14] J. B. Reece, L. A. Urry, M. L. Cain, S. A. Wasserman, P. V. Minorsky, and R. B. Jackson, *Campbell Biology*, 9th ed. (Benjamin Cummings, San Francisco, CA, 2010).
[15] J. Genzer and J. Groenewold, Soft matter with hard skin: From skin wrinkles to templating and material characterization, Soft Matter **2**, 310 (2006).
[16] F. M. Watt and B. L. M. Hogan, Out of eden: Stem cells and their niches, Science **287**, 1427 (2000).
[17] K. A. Moore and I. R. Lemischka, Stem cell and their niches, Science **311**, 1880 (2006).
[18] F. Chowdhury, S. Na, D. Li, Y.-C. Poh, T. S. Tanaka, F. Wang, and N. Wang, Material properties of the cell dictate stress-induced spreading and differentiation in embryonic stem cells, Nat. Mater. **9**, 82 (2010).
[19] H. Babahosseini, A. N. Ketene, E. M. Schmelz, P. C. Robert, and M. Agah, Biomehcanical profile of cancer stem-like/tumor-initiating cells derived from a progressive ovarian cancer model, Nanomed.: NCM **10**, e1013 (2014).
[20] B. Li, Y.-P. Cao, X.-Q. Feng, and H. Gao, Mechanics of morphological instabilities and surface wrinkling in soft materials: A review, Soft Matter **8**, 5728 (2012).
[21] E. Cerda and L. Mahadevan, Geometry and Physics of Wrinkling, Phys. Rev. Lett. **90**, 074302 (2003).
[22] C. O. Flynn and B. A. O. McCormack, A three-layer model of skin and its application in simulating wrinkling, Comput. Methods Biomech. Biomed. Eng. **12**, 125 (2009).
[23] A. R. Hale, Morphogenesis of volar skin in human fetus, Am. J. Anat. **91**, 147 (1952)
[24] W. J. Babler, Embryologic development of epithelial ridges and their configurations, Birth Defects Orig. **27**, 95 (1991).
[25] R. M. Lavker and T. T. Sun, Epidermal stem cells, Adv. Dermatol. **21**, 121 (1983).
[26] B. Li, Y.-P. Cao, X.-Q. Feng, and H. Gao, Surface wrinkling of mucosa induced by volumetric growth: Theory, simulation and experiment, J. Mech. Phys. Solids **59**, 758 (2011).
[27] B. Li, Y.-P. Cao, X.-Q. Feng, and S.-W. Yu, Mucosal wrinkling in animal antra induced by volumetric growth, Appl. Phys. Lett. **98**, 153701 (2011).
[28] A. J. P. Klein-Szanto and H. E. Schroeder, Architecture and density of the connective tissue papillae of the human oral mucosa, J. Anat. **123**, 93 (1975).
[29] P. Ciarletta and A. M. Ben, Papillary networks in the dermal-epidermal junctions of skin: A biomechanical model, Mech. Res. Commun. **42**, 68 (2012).
[30] M. Kuchen and A. C. Newell, Fingerprint formation, J. Theor. Biol. **235**, 71 (2005).
[31] E. Hannezo, J. Prost, and J.-F. Joanny, Instabilities of Monolayered Epithelia: Shape and Structure of Villi and Crypts, Phys. Rev. Lett. **107**, 078104 (2011).
[32] P. Ciarletta, Buckling Instability in Growing Tumor Spheroids, Phys. Rev. Lett. **110**, 158102 (2013).
[33] M. Basan, J.-F. Joanny, J. Prost, and T. Risler, Undulation Instability of Epithelial Tissues, Phys. Rev. Lett. **106**, 158101 (2011).
[34] J. Ovadia and Q. Nie, Stem cell niche structure as an inherent cause of undulating epithelial morphogenesis, Biophys. J. **104**, 237 (2013).
[35] T. Risler and M. Basan, Morphological instabilities of stratified epithelia: A mechanical instability in tumor formation, New J. Phys. **15**, 065011 (2013).
[36] A. D. Lander, K. K. Gokoffski, F. Y.-M. Wan, Q. Nie, and A. L. Calof, Cell lineages and the logic of proliferative control, PLoS Biol. **7**, e1000015 (2009).
[37] E. S. Wu and W. W. Webb, Critical liquid-vapor interface in SF_6. II. Thermal excitations, surface tension, and viscosity, Phys. Rev. A **8**, 2077 (1973).
[38] H. H. Wu, S. Ivkovic, R. C. Murray, S. Jaramillo, K. M. Lyons, J. E. Johnson, and A. L. Calof, Autoregulation of neurogenesis by gdf11, Neuron **37**, 197 (2003).
[39] J. D. Holcomb, J. S. Mumm, and A. L. Calof, Apoptosis in the neuronal lineage of the mouse olfactory epithelium—regulation in-vivo and in-vitro, Dev. Biol. **172**, 307 (1995).
[40] M. L. Manning, R. A. Foty, M. S. Steinberg, and E.-M. Schoetz, Coaction of intercellular adhesion and cortical tension specifies tissue surface tension, Proc. Natl. Acad. Sci. U.S.A. **107**, 12517 (2010).
[41] R. A. Weinberg, *The Biology of Cancer* (Garland Science, New York, 2007).
[42] C.-S. Chou, W.-C. Lo, K. K. Gokoffski, Y.-T. Zhang, F. Y.-M. Wan, A. D. Lander, A. L. Calof, and Q. Nie, Spatial dynamics of multistage cell lineages in tissue stratification, Biophys. J. **99**, 3145 (2010).
[43] E. Hannezo, J. Prost, and J.-F. Joanny, Growth, homeostatic regulation and stem cell dynamics in tissue, J. R. Soc. Interface **11**, 20130895 (2014).
[44] P. Friedl and D. Gilmour, Collective cell migration in morphogenesis, regeneration and cancer, Nat. Rev. **10**, 445 (2009).

[45] L. D. Landau, L. P. Pitaevskii, and E. M. Lifschitz, *Theory of Elasticity*, 3rd ed. (Elsevier Butterworth-Heinemann, Oxford, UK, 1986).

[46] J. H. Kim, L. T. Dooling, and A. R. Asthagiri, Intercellular mechanotransduction during multicellular morphodynamics, J. R. Soc. Interface **7**, S341 (2010).

[47] U. S. Schwarz and S. A. Safran, Elastic Interactions of Cells, Phys. Rev. Lett. **88**, 048102 (2002).

[48] U. S. Schwarz, N. Q. Balaban, D. Riveline, A. Bershadsky, B. Geiger, and S. A. Safran, Calculation of forces at focal adhesions from elastic substrate data: The effect of localized force and the need for regularization, Biophys. J. **83**, 1380 (2002).

[49] I. B. Bischofs, S. A. Safran, and U. S. Schwarz, Elastic interactions of active cells with soft materials, Phys. Rev. E **69**, 021911 (2004).

[50] M. Rauzi and P. F. Lenne, Cortical forces in cell shape changes and tissue morphogenesis, Curr. Topics Dev. Biol. **95**, 93 (2011).

[51] H. Tanimoto and M. Sano, Dynamics of Traction Stress Field During Cell Division, Phys. Rev. Lett. **109**, 248110 (2012).

[52] M. Rauzi, P. Verant, T. Lecuit, and P. F. Lenne, Nature and anisotropy of cortical forces orienting Drosopila tissue morphogenesis, Nat. Cell Biol. **10**, 1401 (2008).

[53] D. M. Bryant and K. E. Mostov, From cells to organs: Building polarized tissue, Nat. Rev. Mol. Biol. **9**, 887 (2008).

[54] T. Bittig, O. Wartlick, A. Kicheva, M. Gonzalez-Gaitan, and F. Julicher, Dynamics of anisotropic tissue growth, New J. Phys. **10**, 063001 (2008).

[55] M. Thery, A. Jimenez-Dalmaroni, V. Racine, M. Bornens, and F. Julicher, Experimental and theoretical study of mitotic spindle orientation, Nature **447**, 493 (2007).

[56] A.-K. Marel, N. Podewitz, M. Zorn, J. Radler, and J. Elgeti, Alignment of cell division axes in directed epithelial cell migration, New J. Phys. **16**, 115005 (2014).

[57] Y. Toyama, X. G. Peralta, A. R. Wells, D. P. Kiehart, and G. S. Edwards, Apoptotic force and tissue dynamics during Drosophila embryogenesis, Science **321**, 1683 (2008).

[58] B. Monier, M. Gettings, G. Gay, T. Mangeat, S. Schott, A. Guarner, and M. Suzanne, Apico-basal forces exerted by apoptotic cells drive epithelium folding, Nature **518**, 245 (2015).

[59] J. Rosenblatt, M. C. Raff, and L. P. Cramer, An epithelial cell destined for apoptosis signals its neighbors to extrude it by an actin- and myosin-dependent mechanism, Curr. Biol. **11**, 1847 (2001).

[60] R. Fernandez-Gonzalez, S. de Matos Simoes, J. C. Roper, S. Eaton, and J. A. Zallen, Myosin II dynamics are regulated by tension in intercalating cells, Dev. Cell. **17**, 736 (2009).

[61] G. T. Mase, R. E. Smelser, and G. E. Mase, *Continuum Mechanics for Engineers*, 3rd ed. (CRC Press, Boca Raton, FL, 2009).

[62] J. Solon, A. Kaya-Copur, J. Colombelli, and D. Brunner, Pulsed forces timed by a ratchet-like mechanism drive directed tissue movement during dorsal closure, Cell **137**, 1331 (2009).